Asian Journal of Water, Environment and Pollution. Vol. 23, No. 1 (2026), pp. 273-292.
doi: 10.36922/AJWEP025380299

ORIGINAL RESEARCH ARTICLE

DNA-intercalation-based selective removal of 1,4,5,8-tetrahydroxy-9,10-anthraquinone *in vitro*

Rongrong Zhang, Junsheng Li*, Guoxia Huang, Liujuan Yan, and Ji Ma

Guangxi Key Laboratory of Green Processing of Sugar Resources, Guangxi University of Science and Technology, Liuzhou, Guangxi, China

***Corresponding author:** Junsheng Li (junshenglee63@aliyun.com)

Received: September 20, 2025; Revised: October 22, 2025; Accepted: October 29, 2025; Published online: November 21, 2025

Abstract: Anthraquinone (AQ) derivatives are persistent environmental pollutants with documented genotoxicity, necessitating efficient methods for their selective removal. This study was therefore designed to characterize the *in vitro* intercalative interaction between THAQ and DNA, determine the binding affinity and thermodynamics, and evaluate DNA-based removal of THAQ. The interaction characteristics of 1,4,5,8-tetrahydroxy-9,10-anthraquinone (THAQ) with DNA *in vitro* were investigated through multiple spectroscopic techniques. Results from ultraviolet-visible spectroscopy, fluorescence spectroscopy, circular dichroism, fluorescence microscopy, and resonance light scattering spectroscopy demonstrated the formation of a stable complex via intercalation of THAQ into the base pairs of DNA *in vitro*. Collectively, these findings indicate an intercalative binding mode between THAQ and free DNA under *in vitro* conditions. DNA thermal denaturation experiments revealed an 8.40°C increase in the melting temperature upon the addition of THAQ, suggesting enhanced stability of the DNA double helix due to intercalation. Fluorescence microscopy indicated that THAQ was selectively adsorbed onto DNA in a manner analogous to the classical intercalator ethidium bromide. The DNA binding saturation value further confirmed strong intercalative binding, with a value of 4.57 for THAQ, significantly higher than those of its analogs (emodin: 0.53, emodin methyl ether: 0.15, and alizarin: 0.19). Under optimal conditions (35°C), the removal efficiency of THAQ by DNA reached 96.67%, in stark contrast to the 3.78% removal achieved by activated carbon. The binding stoichiometry and binding constant were determined to be 0.9479 and 1.4457×10^4 L/mol, respectively. Adsorption kinetics and thermodynamics revealed that the process followed the pseudo-second-order kinetic model ($0.9922 < R^2 < 0.9967$) and the Langmuir isotherm model, with spontaneous binding ($\Delta G < 0$). This study elucidates the interaction mechanisms between THAQ and DNA *in vitro* and proposes a novel strategy for THAQ removal based on DNA intercalation.

Keywords: 1,4,5,8-Tetrahydroxy-9,10-anthraquinone; Herring sperm DNA; Intercalation; Spectroscopy; Magnetic bead separation

1. Introduction

Anthraquinones (AQs) constitute a class of organic compounds characterized by planar structures and high molecular rigidity,[1] featuring an extended conjugated system formed by three fused benzene rings that confers remarkable chemical stability. These compounds, which can be naturally occurring or synthetically produced,[2] are widely utilized as industrial dyes and intermediates in various chemical synthesis processes.[3] Notably, some of their derivatives, such as tetrahydroanthraquinones, display a unique duality: They are recognized as

environmental pollutants while also exhibiting biological activities. For instance, specific tetrahydroanthraquinone derivatives have been documented to inhibit cancer cell proliferation through modulation of key signaling pathways such as phosphoinositide 3-kinase/protein kinase B, suggesting potential biomedical value.[4] Owing to their robust chemical stability, AQs tend to accumulate in the environment, posing substantial carcinogenic, teratogenic, and mutagenic hazards.[5-7] Therefore, establishing highly sensitive detection methods is particularly important. For example, photothermal analysis technology developed based on tetrahydroanthraquinone's coordination properties enables sensitive detection.[8] Meanwhile, developing reliable removal strategies is equally crucial, and adsorption systems constructed using functional materials have been demonstrated to be an effective solution.[9,10] Notably, AQ^2 itself was classified as a Group 2B carcinogen by the International Agency for Research on Cancer in 2017, underscoring its potential risks to human health.

As a prominent derivative within the AQ family, 1,4,5,8-tetrahydroxy-9,10-anthraquinone (THAQ) possesses symmetric hydroxyl substituents at the 1, 4, 5, and 8 positions, a structural feature that endows it with unique chemical properties.[12] As a key intermediate, THAQ is widely applied in multiple domains, including the synthesis of dyes, drugs, and optoelectronic materials, as well as in medical diagnostics.[13] However, accumulating evidence has confirmed its significant genotoxicity,[14] along with its capacity to induce severe dermal and respiratory irritation, leading to its classification as a carcinogen.[15]

The widespread use and environmental release of AQ-based compounds are well-documented. The parent compound, AQ, is a recognized environmental contaminant detected in various matrices such as wastewater, soil, air, and food packaging.[16] More concerningly, AQ has been frequently detected in foodstuffs; for instance, concentrations up to 0.546 mg/kg have been reported in tea, demonstrating its entry into the human food chain.[17] Given that THAQ shares the persistent and stable AQ scaffold and is itself an important industrial intermediate, it poses a potential environmental risk analogous to its parent compound.[18,19] While natural dietary exposure to THAQ remains limited, the expansion of industrial synthesis processes has resulted in increasingly severe environmental contamination.[20]

DNA serves as the principal carrier of genetic information in living organisms and plays an indispensable role in biological transcription and development. Consequently, it constitutes a primary target for both endogenous and exogenous damaging agents. Xenobiotics (such as ultraviolet light, ionizing radiation, and environmental chemicals) and endogenous metabolic byproducts (e.g., reactive oxygen species) can cause a wide array of DNA lesions, including base modifications, strand breaks, and cross-links.[21] If these lesions are not effectively repaired by intricate DNA repair systems (such as nucleotide excision repair and base excision repair), they can be fixed as permanent mutations during cell division.[22] The accumulation of such mutations is a central driving force behind the initiation and progression of cancer, which is why identifying these driver mutations in tumor genomes has become a cornerstone of modern cancer therapeutic development.[23] Therefore, the interactions between DNA and xenobiotics represent a critical initiating event in the pathogenesis of various diseases, including cancer.[24] Planar aromatic compounds can intercalate into DNA base pairs through non-covalent interactions, including π–π stacking, hydrophobic interactions, ionic bonds, hydrogen bonds, and van der Waals forces.[25] Lerman[26] first reported in 1961 that small molecules possessing planar, rigid structures could insert between DNA base pairs. Planar or approximately planar aromatic systems are characteristic features of compounds classified as intercalative DNA binders.[27-31] These intercalator molecules insert their planar aromatic chromophores between adjacent DNA base pairs, a process that can occur both *in vivo* and *in vitro*.[32] Guided by Lerman's intercalation theory, a wide variety of potent DNA intercalating agents have been developed and reported, including acridines, naphthalimides, and AQ compounds.[33-35]

Many AQ derivatives exhibit the typical features of DNA intercalators. Their intercalation can cause localized structural changes to DNA, such as unwinding of the double helix,[36] and after metabolic activation *in vivo* can lead to mutagenic DNA adducts. However, detailed studies on the intercalation mechanisms of specific AQs like THAQ remain scarce.[6] Only once it is confirmed that intercalation can occur between THAQ and free DNA *in vitro* can new methods for the selective removal of THAQ from pollutants through DNA intercalation be explored. In DNA binding studies, herring sperm DNA (hs-DNA) is widely employed.[37] Owing to its abundant availability,[38] low cost,[39] and high purity,[40] it has been chosen as a research material by numerous investigators. Accordingly, hs-DNA was selected as the research material in the present study to investigate the interaction between hs-DNA and THAQ *in vitro*.

Therefore, this study was designed to systematically elucidate the interaction between THAQ and hs-DNA *in vitro* and to explore this interaction for the development of a novel pollutant removal strategy. The specific aims and investigative approach were as follows: First, the binding mode and affinity between THAQ and hs-DNA were rigorously characterized under controlled conditions (in Tris-HCl buffer, pH 7.40) using a suite of spectroscopic and microscopic techniques, including ultraviolet-visible (UV-Vis) spectroscopy, fluorescence spectroscopy, circular dichroism (CD), DNA thermal denaturation analysis, resonance light scattering (RLS), and fluorescence microscopy coupled with magnetic bead separation. These multifaceted approaches, informed by recent insights into small molecule-DNA interactions,[41] allowed for conclusive determination of the intercalative binding mechanism. Second, the thermodynamic parameters were derived to identify the driving forces of the binding interaction. Third, based on confirmed intercalation, we investigated the application of DNA as a selective adsorbent for THAQ removal. The effects of key operational parameters, including contact time, DNA dosage, temperature, and pH, on removal efficiency were systematically evaluated, drawing inspiration from the design of responsive biomaterials.[9] Finally, the process was analyzed in depth using adsorption kinetics and isotherm models to understand the underlying mechanism and assess its practical potential. Collectively, this work establishes a foundational DNA-intercalation-based approach for the selective removal of AQ from pollutants, providing both a theoretical framework and a practical methodology for environmental remediation.

2. Materials and methods

2.1. Chemicals and reagents

The compound THAQ (Shanghai Xianghui Pharmaceutical Technology, China) was first dissolved in 98% ethanol, then diluted with Tris-HCl buffer solution (pH 7.40) and stored in the dark at 4°C. After hsDNA (Solarbio Science and Technology, China) was dissolved in Tris-HCl buffer, the absorbance at 260 nm was measured to calculate the DNA concentration. All chemicals used were of analytical grade and were kept refrigerated at 4°C before use. Enriching Biotechnology Ltd. (China) provided the magnetic beads.

2.2. Instrumentation

A Cary 60 UV-Vis spectrophotometer and a Cary Eclipse fluorescence spectrophotometer (both supplied by Agilent Technologies, United States of America [USA]), an Applied Photophysics Ltd. CD spectrometer (Chirascan CS3016, UK), a DM4B automated fluorescence microscope (Leica Microsystems, Germany), an XW-80A vortex mixer (Shanghai Jingke Industrial, China), and an ISRDV3 constant temperature incubator shaker (Crystal Instruments, USA) were used in the experiments.

2.3. Procedures

2.3.1. Mode of interaction between DNA and THAQ

(a) UV-Vis spectroscopy

All procedures were carried out at room temperature (25°C) in Tris-HCl buffer (pH 7.40). For the forward titration, 3 mL of DNA solution (3.02×10^{-5} mol/L) was placed in a quartz cuvette. Before recording UV-Vis spectra (200–400 nm), THAQ solution (1.60×10^{-4} mol/L) was gradually added in 10 μL increments while being thoroughly mixed and equilibrated for 10 min. Conversely, for reverse titration, 3 mL of THAQ solution was added into the cuvette, with DNA solution added incrementally (10 μL per addition) under identical mixing, equilibration, and spectral scanning conditions.

(b) DNA melting assay

Under pH 7.40 conditions at ambient temperature, a DNA solution and a THAQ-DNA mixture were prepared separately in two cuvettes. Both solutions were heated from 25°C to 100°C in a constant-temperature bath. The absorbance at 260 nm for each solution was measured every 5°C until reaching 100°C. The fraction of single-stranded DNA (f_{ss}) was calculated using Equation (1), and the melting temperature (T_m) of DNA and THAQ-DNA complex was determined from the transition midpoint of the f_{ss} temperature curve:

$$f_{ss} = \frac{A - A_0}{A_f - A_0} \quad (1)$$

Where f_{ss} denotes the extent of DNA unwinding, A is the absorbance at 260 nm measured at various temperatures, the absorption values at 260 nm at 25°C and 100°C are indicated by A_0 and A_f, respectively.

(c) Fluorescence spectroscopy

At pH 7.40 and ambient temperature, a quartz cuvette was filled with 3 mL of THAQ solution. DNA solution was then incrementally added to the cuvette in 10 μL aliquots. After thorough mixing and 10 min of equilibration, the fluorescence

spectrum of THAQ was recorded following each DNA addition. Changes in the fluorescence spectra of THAQ (before and after DNA addition) were analyzed. For the measurements, the scan range was set to 250–500 nm, the excitation wavelength was fixed at 250 nm, the scan speed was selected as "fast," and the slit width was configured to 5.0 nm for both excitation and emission.

(d) CD spectroscopy

CD measurements were performed to assess the influence of THAQ on DNA secondary structure. Under ambient conditions at pH 7.40, DNA solution (6.36×10^{-5} mol/L) was added into five cuvettes, followed by the addition of varying volumes of THAQ solution (0, 50, 150, 200, and 250 μL). The total volume of each mixture was adjusted to 4 mL using Tris-HCl buffer (pH 7.40) and thoroughly mixed on a vortex mixer. The Tris-HCl buffer (pH 7.40) was used as a background reference and subtracted from all DNA-THAQ spectra to ensure that the observed signals originated exclusively from biomolecular interactions. CD spectra were acquired under nitrogen purging over a wavelength range of 200–500 nm, with a time per point of 0.3 s and a bandwidth of 1 nm. Each spectrum represents the average of three consecutive scans.

(e) Fluorescence microscopy with magnetic beads

Initially, 0.1 mL of DNA solution was mixed with 0.5 mL of THAQ solution in a centrifuge tube. The mixture was thoroughly vortex-mixed and then allowed to react at room temperature for 10 min. Subsequently, 0.2 mL of binding buffer and 0.1 mL of magnetic bead suspension were added to the tube, followed by incubation at 40°C with agitation at 300 rpm for 1 h. After incubation, magnetic separation was performed to isolate the beads, and the supernatant was discarded. The beads were washed several times with ethanol, and 1 μL of the bead suspension was finally deposited on a glass slide for observation under a fluorescence microscope.

To evaluate the reliability of the experimental results, control experiments were conducted by incubating magnetic beads directly with ethidium bromide (EB) or THAQ solutions in the absence of DNA. All binding assays were independently repeated in triplicate. Fluorescent spots with comparable intensity and distribution patterns were consistently observed across all three independent replicates, demonstrating high reproducibility of both the intercalative binding between THAQ and DNA and the magnetic bead capture process. Consistent with these findings, no significant fluorescence signals were detected in any of the triplicate DNA-free control groups (where beads were incubated directly with EB or THAQ), thereby excluding interference from non-specific adsorption. The experimental procedure and quality control methodology followed previously validated standards for DNA binding assays.[42]

(f) RLS spectroscopy

At pH 7.40 and room temperature, 3 mL of THAQ solution was added to a quartz cuvette. The RLS spectrum of the Tris-HCl buffer was first recorded as a background reference. The RLS spectrum of THAQ was then acquired using a fluorescence spectrophotometer with both excitation and emission wavelengths set at 250 nm. Subsequently, the DNA solution was incrementally added to the cuvette in 10 μL aliquots. After each addition, the solution was allowed to equilibrate for 10 min to ensure that the binding equilibrium was attained prior to recording the RLS spectrum of THAQ. Spectral changes of THAQ before and after DNA addition were analyzed. The background RLS signal of the buffer was subtracted from all sample spectra, and all measurements were independently repeated in triplicate. The DNA-binding Stern–Volmer (DNABSV), which serves as an indicator of intercalative capacity, was calculated using Equation (2) as follows:

$$DNABSV = \frac{C_{THAQ}}{C_{DNA}} \tag{2}$$

(g) The binding affinity of THAQ for DNA

- Fluorescence quenching by DNA

Fluorescence quenching mechanisms are broadly categorized as static quenching (formation of ground-state complexes) or dynamic quenching (collisional deactivation).[43] To determine the THAQ-DNA quenching type, Stern–Volmer analysis was performed at 25°C, 30°C, and 35°C (Equation [3]):

$$\frac{F_0}{F} = 1 + K_q \tau [Q] = 1 + K_{sv}[Q] \tag{3}$$

Here, F_0 and F represent the fluorescence intensities of THAQ in the absence and presence of DNA,

respectively; K_q is the bimolecular quenching rate constant; and τ_0 (10^{-8} s) refers to the average fluorescence lifetime of the unquenched fluorophore. K_{sv} stands for the Stern–Volmer quenching constant. These values were derived from the linear regression of F_0/F against [Q], where [Q] corresponds to the concentration of DNA.

- The binding constant and binding sites
  The binding between small molecules and biomacromolecules does not follow a 1:1 stoichiometry. To rigorously evaluate THAQ-DNA binding affinity, the binding constant (K_A) and the number of binding sites (n) were determined based on the double logarithmic regression model, as expressed in Equation (4):

$$\log\frac{F_0}{F} = \log K_A + n\log[Q] \tag{4}$$

where n denotes the number of binding sites and K_A is the binding constant.

2.3.2. Adsorption of THAQ by other materials

Activated carbon (0.15 g) was added to a test tube with 5 mL of triple-distilled water and agitated at 300 rpm for 1 h to ensure thorough dispersion. After centrifuging the mixture for 10 min at 10,000 rpm, the supernatant was discarded, and 4 mL of THAQ solution was added. This mixture was agitated at 300 rpm for 120 min at 35°C and pH 7.40. Following incubation, the supernatant was moved to a fresh tube for fluorescence spectroscopic detection of any remaining THAQ after centrifugation at 10,000 rpm for 10 min.

DNA solution (0.8 mL), magnetic beads (0.08 mL), and Tris-HCl buffer (4.12 mL) were combined in a microcentrifuge tube and agitated for 30 min to facilitate DNA adsorption onto beads. After centrifugation at 10,000 rpm for 10 min, the DNA-bead complex was separated and mixed with 4 mL THAQ solution. The mixture was agitated at 300 rpm for 120 min at 35°C and pH 7.40. Following incubation, the sample was centrifuged at 10,000 rpm for 10 min, and the supernatant was collected for quantification of residual THAQ using fluorescence spectroscopy.

Based on characteristic fluorescence peaks measured under each condition, the removal rate R (%) and adsorption capacity q_e (mg/g) of activated carbon and DNA for THAQ were calculated using Equation (5) and Equation (6), respectively:

$$R = \frac{C_0 - C_f}{C_f} \times 100\% \tag{5}$$

$$q_e = \frac{C_0 - C_f \times V}{W} \tag{6}$$

where C_0 is the THAQ initial concentration (mg/L); C_f is the THAQ concentration after adsorption (mg/L); V is the volume of THAQ solution (L); and W is the composite dosage (g).

2.3.3. Adsorption experiments of DNA and THAQ

The effects of contact time (5, 15, 30, 45, 60, 75, and 90 min), DNA dosage (0.523, 1.570, 2.162, 3.363, and 4.710 mg/L), temperature (25, 30, 35, 40, and 45°C) pH (6.60, 7.00, 7.40, 7.80, 8.20, and 8.80), and initial THAQ concentration (0.22, 0.27, 0.54, 0.82, and 1.36 mg/L) on THAQ removal efficiency and DNA intercalative binding were systematically investigated by modulating magnetic bead-mediated DNA-THAQ interactions.

Furthermore, the influences of individual and mixed co-existing substances were comprehensively evaluated. Under the optimized conditions, control experiments were conducted by introducing calcium ions (Ca^{2+}), magnesium ions (Mg^{2+}), potassium ions (K^{+}), vitamin C (VC), D-glucose (Glu), or sodium dodecyl sulfate (SDS) into the reaction system. In addition, to probe potential synergistic or antagonistic effects, mixtures of these substances were also tested, including Ca^{2+} + Mg^{2+}, VC + Glu, SDS + Ca^{2+}, VC + Glu + SDS + Ca^{2+} + Mg^{2+}, and a combined mixture of all additives.

After magnetic capture of DNA-bead complexes, residual THAQ in solution was quantified via fluorescence spectroscopy. THAQ removal efficiency and adsorption capacity were subsequently calculated using Equations (V) and (VI) based on characteristic fluorescence peaks.

2.3.4. Adsorption kinetics, isotherms, and thermodynamic models

Adsorption kinetic models describe the rate and mechanism of the entire adsorption process by describing the adsorption rate through the analysis of temporal variations in adsorption capacity.[44,45] The pseudo-first-order kinetic model Equation (7) and pseudo-second-order kinetic model Equation (8) were employed to characterize THAQ adsorption onto the composite material:

$$ln(q_e - q_t) = lnq_e - K_{1t} \tag{7}$$

$$\frac{t}{q_t} = \frac{1}{K_2 q_e^{\,2}} + \frac{t}{q_e} \tag{8}$$

where K_1 is the rate constant (min^{-1}) for the pseudo-first-order adsorption kinetic model and K_2 is the rate

constant [g·(mg/min)] for the pseudo-second-order adsorption kinetic model, q_t is the quantity of substance adsorbed at point *t* (mg/g), and t is the contact time (min).

The Weber–Morris intraparticle diffusion model ranks as the third most frequently applied model in adsorption kinetics studies, after the pseudo-first-order and pseudo-second-order kinetic models. It was computed using Equation (9) and is used to clarify the rate-limiting stage of the adsorption mechanism:

$$q_t = K_3 t^{0.5} + C \tag{9}$$

Where K_3 is the intraparticle diffusion rate constant (mg/g·min$^{-0.5}$), and C is a constant related to the boundary thickness.

The Langmuir and the Freundlich isotherm models are commonly employed to analyze adsorption isotherm data for determining adsorbent surface properties and adsorption characteristics.[46] The Langmuir model, applicable to homogeneous monolayer adsorption, is seen in Equation (10):

$$\frac{C_e}{q_e} = \frac{C_e}{q_m} + \frac{1}{q_m K_L} \tag{10}$$

Where q_e denotes the adsorption capacity at equilibrium (mg/g), q_m represents the theoretical maximum monolayer adsorption capacity in the Langmuir model (mg/g), C_e refers to the equilibrium concentration in solution (mg/L), and K_L signifies the Langmuir adsorption equilibrium constant (L/mg).

The Freundlich isotherm model is calculated by Equation (11):

$$\ln q_e = \ln K_F + \frac{\ln C_e}{n} \tag{11}$$

Where K_F is the Freundlich isotherm model adsorption equilibrium constant (mg$^{1-1/n}$·L$^{1/n}$·g^{-1}), and *n* is a dimensionless factor.

The Dubinin–Radushkevich (D-R) isotherm model describes the energy of each adsorbent molecule, denoted by ε, as the free energy of adsorption. Physical adsorption occurs when E is <8 kJ/mol, whereas chemical adsorption occurs between 8 and 16 kJ/mol. The D-R isotherm model is represented by Equation (12). Equations (13) and (14) can be used to calculate the average adsorption energy *E* (kJ/mol):

$$\ln q_e = \ln q_s - K_{ad}\varepsilon^2 \tag{12}$$

$$\varepsilon = RT\ln\left(1 + \frac{1}{q_e}\right) \tag{13}$$

$$E = \frac{1}{\sqrt{2K_{ad}}} \tag{14}$$

Where q_s represents the theoretical maximum adsorption capacity (mg/g), K_{ad} is the equilibrium constant of the Dubinin–Radushkevich isothermal model [(mol^2·kJ)$^{-2}$, and ε is the Polanyi potential (mol^2·kJ^{-2}).

The thermodynamic parameters for THAQ-DNA adsorption were examined using adsorption experiments at various temperatures. Equations (15)–(17) were used to calculate ΔH, ΔS, and ΔG:

$$\Delta G = -RT\ln K_A \tag{15}$$

$$\Delta G = \Delta H - T\Delta S \tag{16}$$

$$\ln K_A = \frac{\Delta S}{R} - \frac{\Delta H}{RT} \tag{17}$$

Where ΔG is the Gibbs free energy (kJ/mol), and *R* denotes the ideal gas constant, 8.314 [J·(mol/K)], *T* is the absolute temperature of adsorption (*K*), K_A is the thermodynamic equilibrium constant of adsorption, ΔH is the standard enthalpy change (kJ/mol), and ΔS is the standard entropy change [J·(mol/K)].

3. Results

3.1. Spectroscopic and microscopic characterization of THAQ-DNA interaction

3.1.1. UV-Vis absorption spectral changes

The interaction between THAQ and DNA was initially investigated by UV-Vis spectroscopy. As shown in Figure 1A, the absorption intensity of DNA at 260 nm increased (hyperchromic effect) with the incremental addition of THAQ. In a reverse titration (Figure 1B), the characteristic absorption band of THAQ at 478 nm exhibited a significant decrease in intensity (hypochromic effect) accompanied by a minor red shift (bathochromic shift) upon the addition of increasing concentrations of DNA.

3.1.2. Changes in DNA melting temperature

The thermal denaturation profiles of DNA in the absence and presence of THAQ are shown in Figure 2. The melting temperature T_m was determined to be 68.80 ± 0.1°C for native DNA and 77.20 ± 0.1°C for

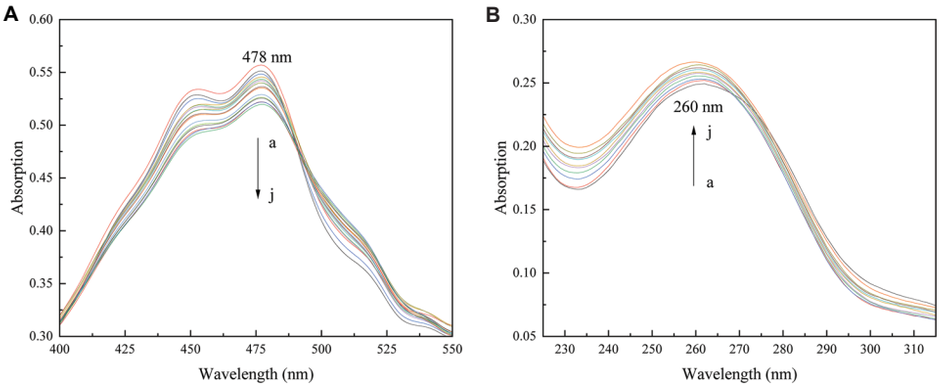

Figure 1. Ultraviolet-visible spectral changes upon THAQ-DNA interaction in Tris-HCl buffer (pH 7.40) at room temperature, (A) [DNA] = 3.02 × 10^{-5} mol/L, a–j: [THAQ] = 0, 0.53, 1.07, 1.60, 2.13, 2.67, 3.20, 3.73, 4.27, 4.80 × 10^{-6} mol/L. (B) [THAQ] = 2.42 × 10^{-5} mol/L, a–j: [DNA] = 0, 0.40, 0.80, 1.20, 1.60, 2.00, 2.40, 2.80, 3.20, 3.60 × 10^{-6} mol/L.

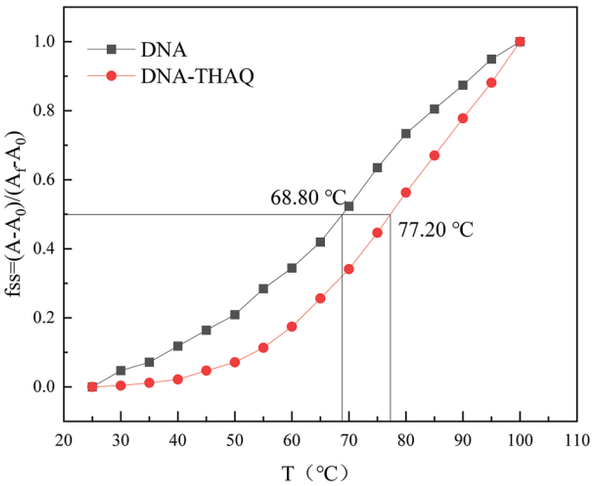

Figure 2. Melting curves of DNA recorded in Tris-HCl buffer (pH 7.40) in the absence and presence of 1,4,5,8-tetrahydroxy-9,10-anthraquinone (THAQ). [DNA] = 6 × 10^{-5} mol/L, [THAQ] = 6 × 10^{-5} mol/L.

the THAQ-DNA complex. The binding of THAQ thus increased the T_m of DNA by approximately 8.40°C.

3.1.3. Fluorescence spectral changes

The intrinsic fluorescence of THAQ was monitored upon the addition of DNA. As shown in Figure 3A, THAQ showed emission peaks at 326 nm and 352 nm. A progressive decrease in fluorescence intensity (fluorescence quenching) was observed as the concentration of DNA increased.

3.1.4. CD spectral changes

The CD spectra of DNA were recorded with increasing concentrations of THAQ (Figure 4). For native B-form DNA, a positive band at 277 nm and a negative band at 249 nm were observed. With the addition of THAQ, the intensity of the positive band gradually decreased, whereas the intensity of the negative band increased.

3.1.5. Fluorescence microscopy observations

Fluorescence microscopy was employed to visually confirm the binding of small molecules to DNA immobilized on magnetic beads. As shown in Figures 5A and C, no fluorescent spots were observed when magnetic beads were incubated directly with EB or THAQ alone. In contrast, distinct fluorescent spots appeared when beads were incubated with the EB-DNA mixture (Figure 5B). Similarly, observable fluorescent spots were present when beads were incubated with the THAQ-DNA mixture (Figure 5D), although the number of spots was lower than with EB.

3.1.6. RLS spectral changes

The RLS spectra of THAQ in the presence of increasing DNA concentrations are presented in Figure 6. THAQ exhibited a distinct RLS peak around 490 nm. The intensity of this RLS peak progressively increased with the addition of DNA and then decreased sharply beyond this concentration. The DNABSV for the THAQ-DNA system, calculated using Equation (II), was determined to be 4.57.

3.1.7. Analysis of fluorescence quenching and binding parameters

(a) Fluorescence quenching by DNA

The fluorescence quenching data were analyzed using the Stern–Volmer equation. The Stern–Volmer plots for the THAQ-DNA system at 25°C, 30°C, and 35°C are presented in Figure 3B. All

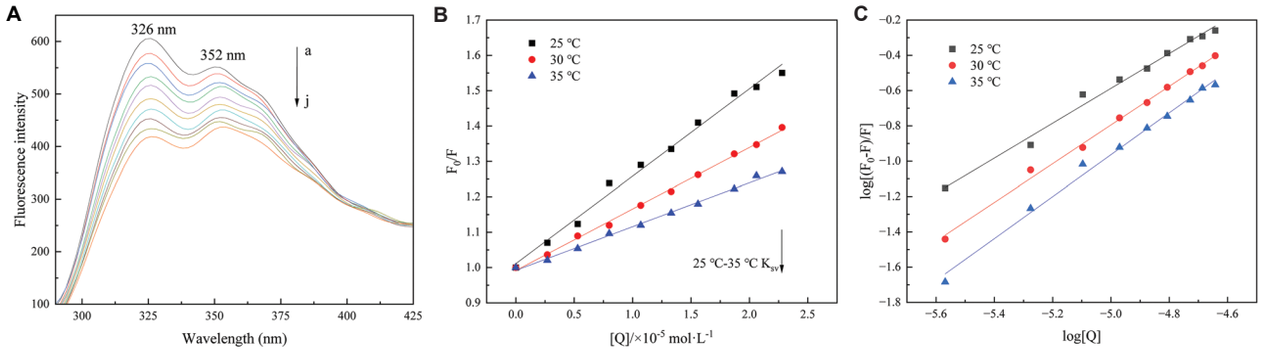

Figure 3. Fluorescence spectroscopy analysis of the 1,4,5,8-tetrahydroxy-9,10-anthraquinone (THAQ)–DNA interaction in Tris-HCl buffer (pH 7.40) at room temperature. (A) Fluorescence emission spectra of THAQ (8×10^{-5} mol/L) with increasing concentrations of DNA (0–2.40×10^{-5} mol/L). (B) Stern–Volmer quenching plots at 25, 30, and 35°C. (C) Double-logarithmic plots for determining the binding constant (K_A) and binding sites (n).

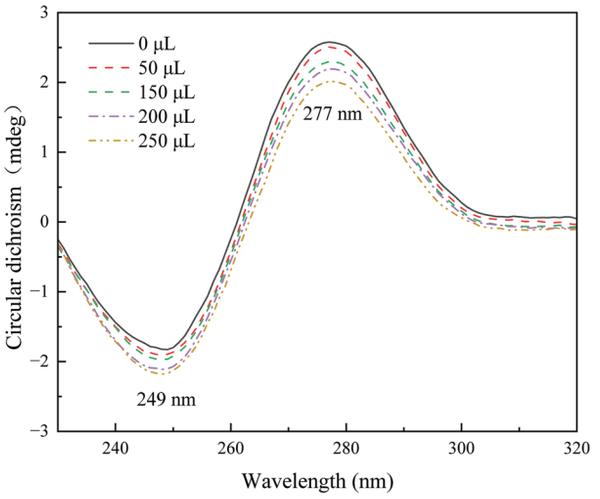

Figure 4. Circular dichroism spectra of DNA in Tris-HCl buffer (pH 7.40) at room temperature, recorded as the concentration of 1,4,5,8-tetrahydroxy-9,10-anthraquinone (THAQ) was gradually raised. [DNA] = 6.36×10^{-5} mol/L, [THAQ] = 0.67, 2.00, 2.67, 3.33 × 10^{-6} mol/L.

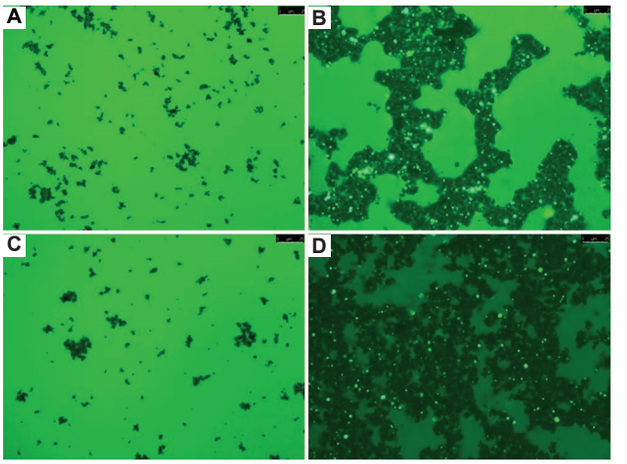

Figure 5. Fluorescence microscopy showing the binding of DNA and small molecules (ethidium bromide [EB] and 1,4,5,8-tetrahydroxy-9,10-anthraquinone [THAQ]) to magnetic beads. Magnetic beads were incubated under the following conditions: (A) EB alone, (B) EB + DNA, (C) THAQ alone, and (D) THAQ + DNA. Scale bars: 25 μm; magnification: 40×.

plots showed good linearity within the studied concentration range. The calculated Stern–Volmer quenching constants (K_{sv}) and bimolecular quenching rate constants (K_q) at these temperatures are summarized in Table 1.

(b) Binding constant and number of binding sites

The double-logarithmic regression curves for the interaction between THAQ and DNA at 25°C, 30°C, and 35°C are shown in Figure 3C. The binding constants (K_A) and binding sites (n) were determined from the slopes and intercepts of these curves. As summarized in Table 1, the binding constants at 25°C, 30°C, and 35°C were calculated to be 1.4457×10^4 mol/L, 1.0231×10^4 mol/L, and 8.3714×10^3 mol/L, respectively. The corresponding numbers of binding sites (n) were 0.9479, 1.0960, and 0.9755.

3.2. Adsorption of THAQ by other materials

Under conditions of initial THAQ concentration (0.27 mg/L), DNA concentration (3.36 mg/L), 35°C, and pH 7.40 with 75 min reaction time, the THAQ adsorption efficiency exceeded 95%. In contrast,

Table 1. Fluorescence quenching and binding parameters for the interaction between 1,4,5,8-tetrahydroxy-9,10-anthraquinone (THAQ) and DNA at different temperatures

Reagent	T (°C)	Stern–Volmer quenching			Double-logarithmic analysis		
		K_{sv} (L/mol)	K_q (L·(mol/s))	R^2	K_A (L/mol)	n	R^2
THAQ	25	2.4729×10^4	2.4729×10^{12}	0.9900	1.4457×10^4	0.9479	0.9914
	30	1.7401×10^4	1.7401×10^{12}	0.9974	1.0231×10^4	1.0960	0.9996
	35	1.2371×10^4	1.2371×10^{12}	0.9953	8.3714×10^3	0.9755	0.9950

Note: R^2 is the coefficient of determination for the linear regression.

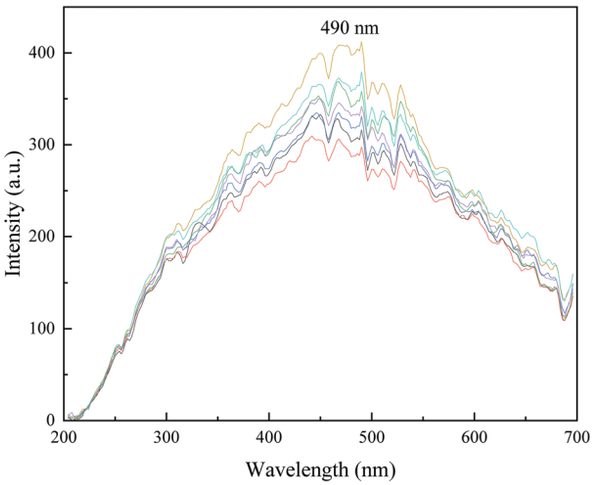

Figure 6. Resonance light scattering spectra of 1,4,5,8-tetrahydroxy-9,10-anthraquinone (THAQ) in Tris-HCl buffer (pH 7.40) at room temperature, recorded in the absence and presence of DNA. (THAQ) = 8.14 × 10^{-6} mol/L, a–g: (DNA) = 0, 0.35, 0.70, 1.05, 1.40, 1.75, 2.10 × 10^{-7} mol/L.

activated carbon achieved only 3.78% adsorption efficiency under identical conditions.

3.3. Adsorption performance of DNA for THAQ

3.3.1. Effect of contact time

As shown in Figure 7A, rapid THAQ removal occurred within the first 15 min under conditions of 35°C and pH 7.40 using DNA-modified magnetic nanoparticles, and adsorption reached equilibrium after 75 min. Removal efficiencies reached 93.85%, 95.34%, 92.62%, 91.92%, and 91.46% at initial THAQ concentrations of 0.22, 0.27, 0.54, 0.82, and 1.36 mg/L, respectively. Beyond 75 min, removal efficiency changed minimally as adsorption approached equilibrium. Thus, 75 min was determined as the optimal adsorption duration.

3.3.2. Effect of DNA dosage

As shown in Figure 7B, the removal efficiency of THAQ decreased from 94.84% to 76.59% as its initial concentration was increased from 0.22 mg/L to 1.36 mg/L.

3.3.3. Effect of varying temperature

According to Figure 7C, the removal efficiency of THAQ was observed to increase with temperature from 20°C to 40°C, beyond which a decrease was noted. The optimal removal efficiencies of 93.24%, 90.30%, and 84.78% were achieved at 35°C for initial THAQ concentrations of 0.27, 0.054, and 0.082 mg/L, respectively.

3.3.4. Effect of varying pH

As shown in Figure 7D, the optimal THAQ removal efficiency was achieved at a neutral pH of 7.40, whereas both acidic and alkaline conditions resulted in reduced efficacy.

3.3.5. Effect of individual co-existing substances

As shown in Figure 7E, individual co-existing substances significantly affected THAQ removal efficiency. Compared to the control group (94.7%), the addition of Ca^{2+} and Mg^{2+} resulted in removal efficiencies of 88.3% and 89.7%, respectively, indicating a moderate inhibitory effect. A slight inhibition was also observed with K^+ (90.2%). In contrast, the introduction of VC and Glu led to a notable enhancement in removal efficiency, which increased to 97.7% and 96.2%, respectively. However, SDS produced the greatest inhibitory effect, which dropped drastically to 83.3%.

3.3.6. Effect of mixed co-existing substances

The removal efficiency of THAQ was further investigated in the presence of mixed co-existing substances, as presented in Figure 7F. The combination of Ca^{2+} and Mg^{2+} showed a strong synergistic inhibitory effect, with efficiency decreasing to 86.2%. Conversely, the mixture of VC and Glu exhibited a significant synergistic enhancement, achieving a removal efficiency of 97.6%. When SDS was combined with Ca^{2+}, a severe antagonistic effect was observed, resulting in a substantially reduced efficiency of 81.0%.

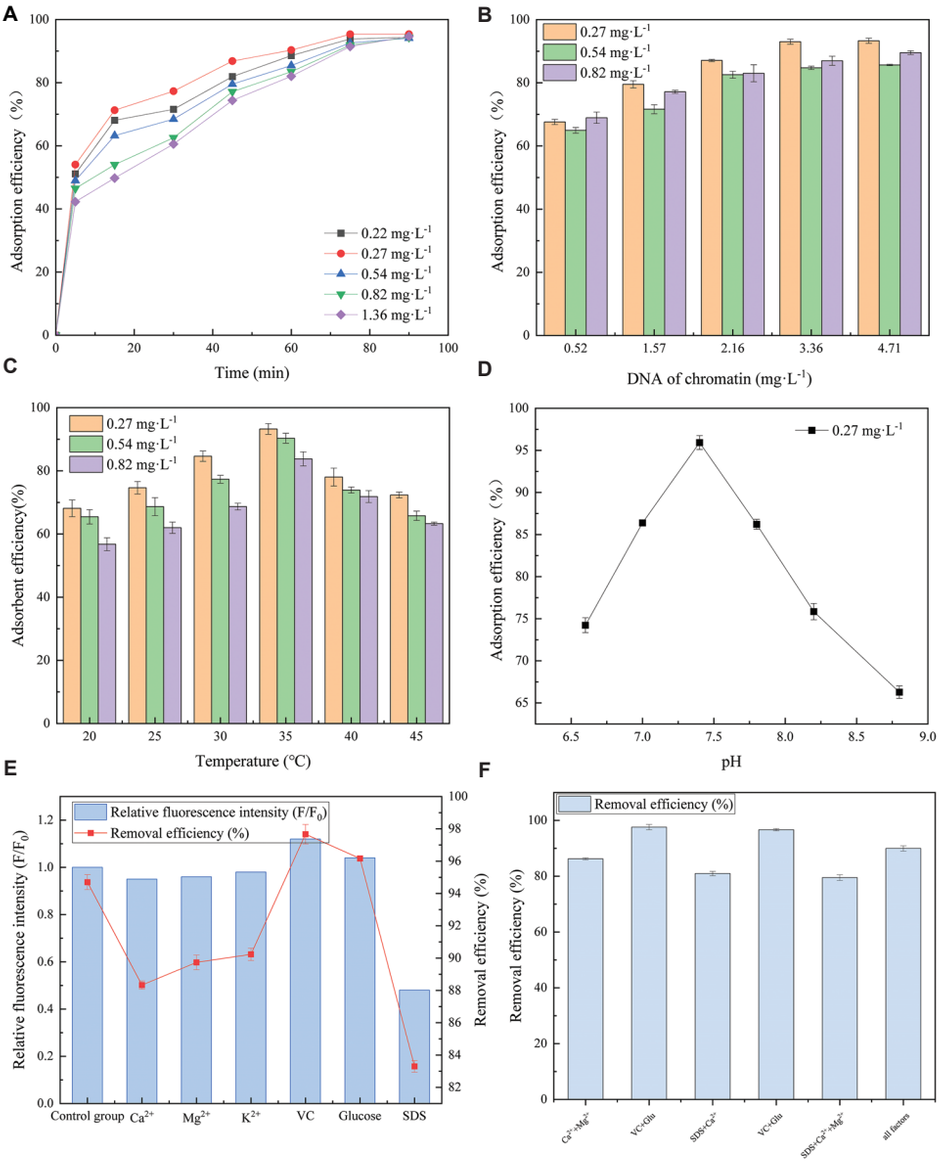

Figure 7. Effects of operational parameters on 1,4,5,8-tetrahydroxy-9,10-anthraquinone (THAQ) adsorption by DNA under various initial concentrations. (A) Contact time, (B) DNA dosage, (C) temperature, (D) solution pH, (E) individual co-existing substances, and (F) mixed co-existing substances.

The combination of VC, Glu, and SDS also led to a substantial inhibition, with an efficiency of 79.5%. Interestingly, the combination of VC, Glu, SDS, Ca^{2+}, and Mg^{2+} yielded a high efficiency of 96.7%. However, when all tested substances were present together, the removal efficiency was 90.0%, closely similar to the control group.

3.4. Analysis of adsorption mechanisms

3.4.1. Adsorption kinetics

Figure 8A and B present the fitting curves of the pseudo-first-order and pseudo-second-order kinetic models for THAQ adsorption onto DNA, with the corresponding kinetic parameters listed in Table 2. Higher correlation coefficients were obtained for the pseudo-second-order model compared to the pseudo-first-order model. The plots of qt versus $t^{0.5}$ from the intraparticle diffusion model (Figure 8C; Table 3) did not pass through the origin.

3.4.2. Adsorption isotherms

The isotherm fitting curves are presented in Figure 9A and B, with the corresponding parameters listed in Table 3. The Langmuir model exhibited higher

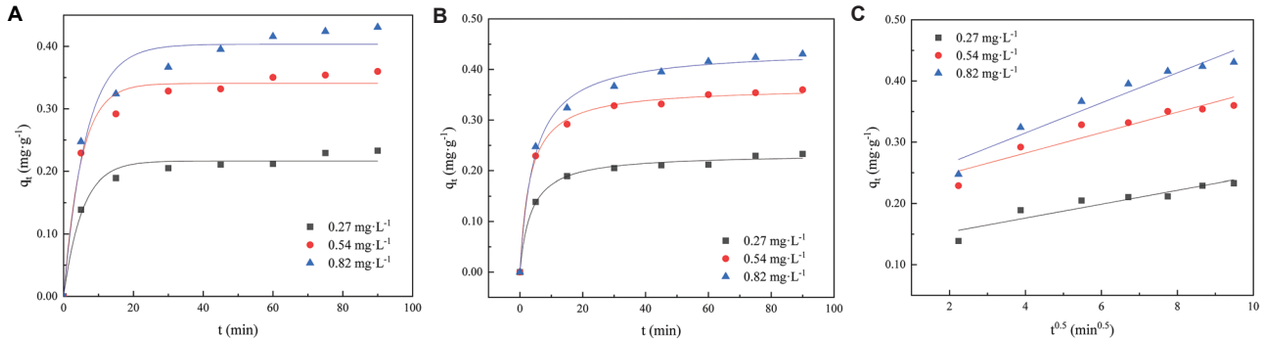

Figure 8. Adsorption kinetics and mechanism. (A) Pseudo-first-order kinetic model, (B) pseudo-second-order kinetic model, and (C) intraparticle diffusion model.

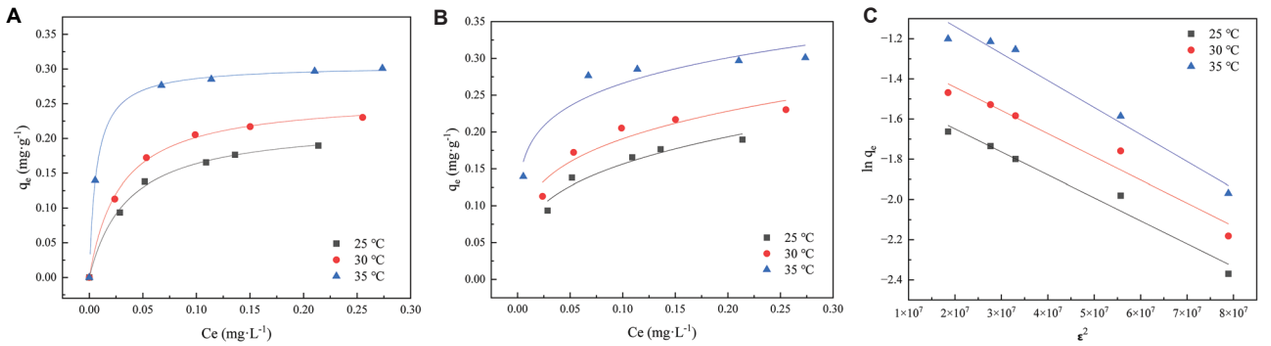

Figure 9. Adsorption isotherm modeling for 1,4,5,8-tetrahydroxy-9,10-anthraquinone (THAQ) removal by DNA. (A) Langmuir isotherm model, (B) Freundlich isotherm model, and (C) Dubinin–Radushkevich isotherm model.

Table 2. Parameters of kinetic models for 1,4,5,8-tetrahydroxy-9,10-anthraquinone (THAQ) adsorption onto DNA

THAQ (mg/L)	Pseudo-first-order kinetic			Pseudo-second-order kinetic			Intraparticle Diffusion Model		
	K_1	q_e	R^2	K_1	q_e	R^2	K_1	q_e	R^2
0.27	0.1095	0.4079	0.9760	1.2216	0.2330	0.9934	0.2167	0.025	0.9258
0.54	0.1892	0.3389	0.9767	0.8581	0.3652	0.9967	0.2153	0.0167	0.8663
0.82	0.1834	0.2181	0.9608	0.5061	0.4407	0.9922	0.1309	0.0113	0.8521

Note: K_1 (min^{-1}); K_2 (g/mg·min^{-1}); K_3 (mg/g·min$^{-0.5}$); q_e (mg/g).

Table 3. Parameters of adsorption isotherm models for 1,4,5,8-tetrahydroxy-9,10-anthraquinone (THAQ) removal by DNA

Temperature (°C)	Langmuir isotherm model			Freundlich isotherm model			Dubinin–Radushkevich isotherm model			
	K_L	q_m	R^2	n	K_F	R^2	K_{ad} (10^{-8})	q_s	R^2	E
25	27.92	0.222	0.9831	3.258	0.3169	0.9136	−1.14	0.242	0.9624	0.662
30	34.77	0.259	0.9907	3.867	0.3460	0.8690	−1.15	0.715	0.9415	0.659
35	150.9	0.305	0.9984	5.656	0.3998	0.8773	−1.34	0.331	0.9592	0.610

Note: K_L (L/mg); q_m (mg/g); K_{ad} (mol^2·kJ^{-2}); q_s (mg/g); E (kJ/mol).

correlation coefficients than the Freundlich model across the studied temperatures. Furthermore, the theoretical monolayer adsorption capacities (q_m) derived from the Langmuir model were in close agreement with the experimentally measured values. The fitting of the D-R model is shown in Figure 9C, and the relevant

parameters are provided in Table 3. The calculated mean adsorption energy (E) values were ≤3.44 kJ/mol.

3.4.3. Thermodynamic parameters

The thermodynamic parameters for the THAQ-DNA interaction *in vitro* are summarized in Table 4. As shown, the values of standard enthalpy change (ΔH) were negative, whereas standard entropy change (ΔS) was positive. The Gibbs free energy change (ΔG) was found to be negative at all studied temperatures.

4. Discussion

4.1. Elucidation of the THAQ-DNA intercalative binding mode

4.1.1. UV-Vis spectral analysis

The hyperchromic effect in the DNA absorption band is closely related to structural changes, suggesting that the binding of THAQ molecules may induce conformational alterations in the DNA double helix.[47] The hypochromicity and red shift in THAQ's absorption band suggest π–π stacking between its aromatic rings and DNA base pairs, thereby reducing the energy and probability of π–π* transitions. Theoretically, both hyperchromism with blue shift and hypochromism with red shift are associated with intercalative binding modes. However, the relatively weak hypochromic and bathochromic shifts observed in the THAQ-DNA system suggest that further investigation is required to conclusively determine their specific interaction mode *in vitro*.

4.1.2. DNA melting profiles

The thermal denaturation temperature is closely related to the structural stability of DNA. Investigating changes in the DNA melting temperature (T_m) before and after interaction with small molecules serves as a reliable method for determining the binding mode.[48] Double-stranded DNA exhibits a significantly lower extinction coefficient at 260 nm than single-stranded DNA; consequently, helix unwinding during thermal denaturation causes progressive hyperchromicity at this wavelength.[49] In this study, the binding of THAQ increased the T_m of DNA by approximately 8.40°C. This pronounced stabilization originates from the insertion of planar aromatic molecules between the DNA base pairs, which effectively enhances the stability of the double-stranded structure against thermal denaturation.[50] Intercalative binding typically increases the DNA T_m by at least 5–8°C whereas groove binding or electrostatic attraction causes negligible changes in T_m. Therefore, the ΔT_m value observed in our experiment provides compelling evidence for the occurrence of intercalative binding between THAQ and DNA *in vitro*.

Table 4. Thermodynamic parameters of 1,4,5,8-tetrahydroxy-9,10-anthraquinone (THAQ)–DNA interaction at three temperatures

Reagent	T (K)	ΔH (KJ/mol)	ΔS (J/mol/K)	ΔG (KJ/mol)
THAQ	298	–	–	−27.93
	303	−21.40	21.91	−28.04
	308	–	–	−28.15

4.1.3. Fluorescence spectral analysis

Fluorescence spectroscopy is routinely used to investigate changes in fluorescence properties before and after small-molecule-DNA interactions.[51] DNA exhibits an extremely low fluorescence quantum yield and is virtually non-fluorescent.[52] Any increase or decrease in fluorescence intensity upon interaction with small molecules indicates binding to DNA.[53] The fluorescence quenching observed in this study is attributed to the intercalation of THAQ molecules between DNA base pairs, where the restricted molecular motion and altered microenvironment of the THAQ chromophore promote non-radiative decay pathways. Combined with preceding experimental evidence, this quenching phenomenon further confirms the formation of THAQ-DNA complexes through intercalative binding.

4.1.4. CD

CD spectroscopy provides an effective approach for monitoring DNA conformational alterations, as CD signals are highly sensitive to environmental perturbations and ligand-binding modes.[54] DNA, being an optically active biomacromolecule, displays two characteristic CD bands in its B form spectrum: a positive peak around 277 nm arising from base stacking interactions, and a negative peak near 249 nm corresponding to right-handed helical conformation. Groove binding or electrostatic interactions induce negligible peak alterations,[55] whereas intercalative binding causes substantial changes in both peak position and intensity. The observed attenuation of the positive band and enhancement of the negative band in this study suggest that THAQ disrupts base-base interactions, reduces stacking density, and may enhance DNA helicity. These characteristic alterations confirmed the occurrence of THAQ-DNA intercalation *in vitro*.

4.1.5. Fluorescence microscopy

The absence of fluorescence when magnetic beads were incubated directly with EB or THAQ confirms negligible non-specific adsorption of these molecules to the beads themselves.[56,57] The appearance of distinct fluorescent spots exclusively in the presence of DNA demonstrates the critical role of DNA in mediating the binding and subsequent magnetic capture. The intense fluorescence observed with the classical DNA intercalator EB served as a robust positive control, validating the experimental setup. The fluorescent spots were observed, although fewer in number, in the THAQ-DNA sample, providing direct visual evidence that THAQ intercalated with DNA *in vitro*, forming complexes that are efficiently captured by the magnetic beads. The lower spot count compared to EB indicates a lower intercalation efficiency or binding affinity of THAQ under the given conditions, a finding consistent with previous quantitative analyses. This methodology effectively combines the separation convenience of magnetic beads with direct visual confirmation of binding, thereby providing compelling support for the intercalation mechanism.[58]

4.1.6. RLS

RLS spectroscopy is highly sensitive to structural alterations induced by small-molecule-biomacromolecule interactions and is widely employed to characterize binding processes, particularly between aromatic compounds and DNA.[59] Given the negligible intrinsic RLS signal of DNA and corroborating evidence from previous binding-mode studies, the enhancement in RLS intensity is attributed to the intercalation of THAQ molecules into DNA base pairs, forming larger THAQ-DNA complexes that amplify scattering signals. The subsequent sharp decrease in intensity beyond a critical concentration indicates saturation of binding sites. The classical DNA intercalator EB exhibits an exceptionally high DNABSV of 14.70. For comparison, the DNABSV values for chrysophanol, physcion, and alizarin are 0.53, 0.15, and 0.19, respectively, all substantially lower than that of EB. The DNABSV of 4.57 obtained for THAQ in this study, though lower than EB, is significantly higher than those of the aforementioned small molecules. This demonstrates that THAQ exhibits strong intercalative binding to DNA *in vitro*, providing a theoretical basis for utilizing DNA to selectively remove THAQ.

The strong intercalative binding affinity of THAQ observed herein, compared to its analogs, underscores its unique molecular recognition properties. It is worth noting that such tetrahydroanthraquinones may provide a mechanistic advantage, as their disrupted conjugated system differs from the redox-active, fully planar AQs, which often cause severe side effects through non-specific DNA damage.[4] This distinction is crucial when considering the application of THAQ-DNA interaction for selective removal, as it suggests a more controlled and selective binding interaction.

4.1.7. Analysis of binding parameters and thermodynamics

(a) Fluorescence quenching mechanism

The fluorescence quenching of THAQ by DNA *in vitro* occurs via a static quenching mechanism. This definitive assignment is supported by the following key evidence: the strong linearity of the Stern–Volmer plots indicates a single quenching process; the inverse correlation between the quenching constant (K_{sv}) and temperature is characteristic of static quenching; and crucially, the calculated bimolecular quenching constants (K_q), on the order of 10^{12} L/mol/s, exceed the maximum value for a diffusion-controlled process by two orders of magnitude, thereby ruling out dynamic quenching. The collective data confirm the formation of a nonfluorescent ground-state complex between THAQ and DNA.

(b) The binding constant and binding sites

This study demonstrates that THAQ and DNA form a stable 1:1 complex *in vitro*, consistent with static quenching behavior. The interaction is characterized by moderate-to-strong binding affinity and an exothermic process. Collectively, the binding constant, thermodynamic profile ($\Delta H < 0$), and the well-defined 1:1 binding stoichiometry provide compelling evidence supporting the conclusion that THAQ binds to DNA through an intercalative mode. These findings clearly define the fundamental characteristics of the THAQ-DNA interaction and establish a solid theoretical foundation for its potential application in pollutant removal.

4.2. Enhanced THAQ adsorption by DNA over activated carbon

The remarkable disparity in adsorption efficiency between DNA-modified materials and activated carbon fundamentally stems from their distinct adsorption mechanisms. Activated carbon primarily relies on its extensive specific surface area for physisorption, a non-specific process that demonstrates limited effectiveness in capturing specific molecules like THAQ. In contrast, the superior performance of the DNA-based adsorbent

is attributed to the specific intercalative binding between THAQ molecules and DNA base pairs. This molecular recognition mechanism, analogous to a "lock-and-key" interaction, enables the selective capture of THAQ molecules from the aqueous phase, forming stable DNA-THAQ complexes.

The optimal conditions identified in this study (35°C, pH 7.40, 75 min) further support the biomolecular interaction mechanism. The neutral pH environment maintains the structural integrity of the DNA double helix, while the moderate temperature enhances molecular diffusion without causing DNA denaturation. Particularly noteworthy is the 95% removal efficiency achieved by DNA-modified materials under these conditions, which not only confirms the high efficiency of intercalative binding but also highlights its unique advantage in treating low-concentration organic pollutants.

From an application perspective, this biomolecular-recognition-based adsorption strategy provides novel insights for the selective removal of recalcitrant organic pollutants. Compared to conventional adsorbents, DNA-modified materials demonstrate significant advantages in specificity, adsorption capacity, and operational conditions, thereby establishing a theoretical foundation for developing advanced water treatment technologies.

4.3. Optimization of adsorption conditions and mechanistic analysis

4.3.1. Effect of contact time

The adsorption process was rapid within the first 15 min, gradually approached equilibrium, and reached saturation at 75 min. The initial fast adsorption is attributable to the abundance of available intercalation sites on the adsorbent surface.[60] As the sites were progressively occupied, the driving force diminished, leading to equilibrium, a behavior consistent with the pseudo-second-order kinetic model for typical surface adsorption processes.[61] The 75-min equilibrium time identified in this study is comparable to or faster than other DNA-based adsorbents reported for similar aromatic compounds, highlighting the potential efficiency of our method in practical applications.

4.3.2. Effect of DNA dosage

The decrease in removal efficiency with increasing initial THAQ concentration directly reflects the limited availability and subsequent saturation of DNA intercalation sites. The high site-to-molecule ratio at lower THAQ concentrations facilitated efficient adsorption, whereas site saturation at higher concentrations reduced the binding probability for additional molecules, thereby diminishing the overall removal efficacy.

4.3.3. Effect of temperature

Temperature modulated the adsorption process by influencing molecular kinetic energy and adsorbent capacity. The increase in removal efficiency below 35°C resulted from enhanced molecular diffusion and adsorption capacity. However, the decline in efficiency beyond the optimal temperature of 35°C is likely due to accelerated molecular motion and increased solubility, potentially inducing THAQ desorption.

4.3.4. Effect of pH

The optimal removal efficiency at physiological neutral pH (7.40) and the decline under both acidic and alkaline conditions are primarily due to alterations in DNA conformation and electrostatic interactions. The elevated H^+ concentration under acidic conditions induces protonation of the phosphate groups, impairing adsorption performance. Conversely, abundant OH^- ions under alkaline conditions weaken the electrostatic attraction between DNA and THAQ molecules. Consequently, deviations from neutral pH disrupt the optimal binding environment.

4.3.5. Effect of individual co-existing substances

The presence of individual co-existing substances exerted varying degrees of influence on the THAQ removal efficiency, which can be correlated with their impact on the intercalative binding environment and the physicochemical state of THAQ. The moderate reduction in efficiency observed with Ca^{2+} and Mg^{2+} may be attributed to their charge-shielding effect. These divalent cations can neutralize the negative charge of the DNA phosphate backbone, potentially compressing the double helix and slightly hindering the intercalation of THAQ. The minimal effect of K^+ is consistent with the weaker perturbation of monovalent ions on DNA structure at the studied concentration. In stark contrast, the most dramatic inhibition caused by SDS is likely due to a dual mechanism: SDS may directly interact with THAQ molecules, quenching their fluorescence and forming complexes that preclude intercalation; simultaneously, SDS micelles could encapsulate THAQ, effectively sequestering it from the DNA binding sites. This significant suppression underscores the high sensitivity of the intercalation-based removal process to surfactant interference. Conversely, the remarkable enhancement caused by VC and Glu suggests that these

molecules might stabilize the DNA-THAQ complex, alter the solvation shell in a way that favors binding, or modify the conformation of THAQ to enhance its planarity and intercalation potential.

4.3.6. Effect of mixed co-existing substances

The effects of mixed substances revealed more complex, non-additive interactions, highlighting intriguing synergistic and antagonistic behaviors. The strong synergistic inhibition observed with the Ca^{2+} and Mg^{2+} mixture suggests their charge-shielding effects on DNA structure are additive, leading to a greater collective hindrance to intercalation than when present alone. Conversely, the synergistic enhancement between VC and Glu indicates a cooperative mechanism in promoting THAQ binding, potentially creating a more favorable microenvironment for the DNA-THAQ interaction. The severe antagonism in the SDS and Ca^{2+} mixture, resulting in the lowest efficiency, might arise from a complex interplay where Ca^{2+} potentially disrupts SDS micelle formation without eliminating its quenching effect, leading to a state that is highly detrimental to binding. The profound inhibition by the VC + Glu + SDS mixture suggests that the promoting effects of VC and Glu cannot overcome the dominant, disruptive influence of SDS in this ternary system. Interestingly, the high efficiency restored in the complex mixture of VC, Glu, SDS, Ca^{2+}, and Mg^{2+} implies that the strong promoting effects of VC and Glu can, under these specific conditions, counteract the inhibitory effects of SDS and divalent cations, possibly through the formation of a new equilibrium or complex interactions that favor DNA binding. Finally, the net neutral effect when all factors were combined suggests a dynamic equilibrium where all promoting and inhibiting forces effectively balance each other, resulting in a removal efficiency indistinguishable from the control system.

4.4. Mechanistic and thermodynamic analysis

A comprehensive analysis of the adsorption kinetics, isotherms, and thermodynamics collectively elucidates the mechanism and nature of THAQ adsorption onto DNA-modified magnetic nanoparticles.

The kinetic study indicated that the adsorption process was better fitted by the pseudo-second-order model, suggesting that the rate may be controlled by a chemisorption mechanism, consistent with the chemical process of intercalative binding between THAQ and DNA. The fact that the intraparticle diffusion plots did not pass through the origin further indicated that surface adsorption and boundary layer diffusion were significant initial rate-limiting steps.

Isotherm modeling demonstrated that the Langmuir model provided the best fit for the adsorption data, indicating monolayer adsorption on a homogeneous surface,[62] which corresponds to the finite and uniformly distributed intercalation sites on the DNA double helix. Meanwhile, the mean adsorption energy ($E \leq 3.44$ kJ/mol) determined from the Dubinin–Radushkevich model falls within the recognized range for physisorption ($E < 8$ kJ/mol).

Thermodynamic parameters provided key insights into the driving forces of the binding. The negative value of ΔG confirms the spontaneous nature of the THAQ-DNA complex formation. The observed negative ΔH and positive ΔS together suggest that the binding process is an exothermic reaction primarily driven by enthalpy. The negative enthalpy change likely originates from the energy released through the formation of strong intermolecular forces (e.g., π–π stacking) associated with intercalation, whereas the positive entropy change may be attributed to the release of bound water molecules and/or counterions from the DNA helix upon THAQ binding.

In summary, the adsorption of THAQ onto the DNA-modified magnetic nanoparticles is a spontaneous, exothermic, and enthalpy-driven physical process, characteristic of monolayer coverage on homogeneous sites. This strongly supports the proposed intercalation mechanism wherein THAQ inserts into DNA base pairs via physical π–π stacking interactions.

4.5. Prospects for practical application and post-removal handling

The high removal efficiency demonstrated herein underscores the potential of DNA-based materials for the sequestration of specific aromatic pollutants. For any adsorption-based remediation technology, the ultimate fate of the pollutant-laden adsorbent is a critical consideration for its environmental sustainability and practical application.[63,64] In the present system, the THAQ is not merely adsorbed but is stably intercalated within the DNA double helix, as confirmed by the significant increase in melting temperature (ΔT_m = 8.40°C and the spontaneous, exothermic nature of the binding (ΔG < 0). This strong interaction significantly reduces the risk of rapid desorption and release of THAQ into the environment.

Moreover, the integration with magnetic bead separation provides a pivotal advantage for post-removal handling. This process effectively transfers

THAQ from a dissolved state in a large aqueous volume to a concentrated and immobilized form on a solid support (the DNA-magnetic bead complex), which is readily separable from the treated water. This fundamental design transforms the challenge from one of managing a dilute aqueous contaminant to one of managing a localized solid waste, for which established and efficient treatment protocols exist.

Several viable pathways can be envisaged for the final treatment of the spent THAQ-DNA-bead complexes:

(i) Thermal treatment: The complexes can be subjected to controlled incineration. The inorganic magnetic core confers stability, whereas the organic components (DNA and THAQ) are completely mineralized at high temperatures.

(ii) Advanced oxidation processes (AOPs): The magnetically harvested slurry presents a concentrated target for AOPs such as Fenton oxidation or ozonation. The treatment efficiency for this small volume, high-concentration stream is anticipated to be substantially higher and more economical than for the original wastewater.

(iii) Enzymatic digestion and resource recovery (a future perspective): A more sophisticated, green chemistry approach could employ nucleases (e.g., DNase I) to selectively hydrolyze the DNA scaffold. This could release THAQ in a concentrated form for potential recovery or targeted catalytic degradation, while simultaneously allowing for the regeneration and reuse of the magnetic beads.

Therefore, the technology presented not only achieves highly selective and efficient removal of THAQ but also, through its design, facilitates the subsequent safe disposal or potential resource recovery of the captured pollutant. This work establishes a foundational strategy for developing practical and environmentally responsible DNA-based remediation technologies.

5. Conclusion

The present study represents the first investigation of the *in vitro* interaction between THAQ and DNA. UV-Vis absorption spectroscopy revealed hyperchromicity and a slight blue shift at DNA's 260 nm characteristic peak, indicating structural alterations in the DNA double helix. Conversely, adding DNA to the THAQ solution caused hypochromicity with a minor red shift in THAQ's spectrum. Both hyperchromicity/blue shift and hypochromicity/red shift signify intercalative binding, suggesting potential intercalation.

DNA melting experiments showed Tm values of 68.80 ± 0.1°C (native DNA) and 77.20 ± 0.1°C (THAQ-DNA complex). The 8.40°C increase confirms DNA stabilization through intercalation. Fluorescence spectroscopy confirmed that DNA quenches THAQ fluorescence.

CD detected concentration-dependent perturbations: the positive band at 277 nm weakened, whereas the negative band at 249 nm intensified, confirming intercalation-induced conformational changes. Magnetic bead adsorption assays with EB control provide visual evidence of THAQ intercalation with DNA.

RLS experiments revealed that DNA progressively enhanced the RLS signal of the THAQ-DNA system within a certain concentration range until binding saturation was achieved. The calculated binding saturation value was 4.57. Compared to 1,2-benzanthracene, chrysophanol, physcion, and alizarin, THAQ exhibited a higher DNABSV, supporting strong intercalative binding with DNA *in vitro*.

Interaction strength was quantified via Stern–Volmer analysis, confirming static quenching through THAQ-DNA complex formation. At 25°C the binding constant (K_A) was 1.4457×10^4 L/mol with a binding stoichiometry (n) of 0.9479. Thermodynamic parameters demonstrated spontaneous, enthalpy-driven complex formation.

At an initial THAQ concentration of 0.27 mg/L, using a DNA solution with a concentration of 3.36 mg/L at 35°C and pH 7.40 for 75 min, its THAQ adsorption efficiency exceeded 95%. By contrast, the THAQ adsorption efficiency was 3.78% for activated carbon. DNA's adsorption of THAQ followed the pseudo-second-order kinetic model ($0.9922 \leq R^2 \leq 0.9967$) and the Langmuir isotherm model ($0.9831 \leq R^2 \leq 0.9984$), indicating homogeneous adsorption on the adsorbent surface. The Dubinin–Radushkevich isotherm model demonstrated that a physical adsorption mechanism was involved in THAQ adsorption by DNA. The intraparticle diffusion model indicated that other mechanisms also affected the adsorption process. Thermodynamic parameters confirmed the spontaneity of the adsorption process. The above results indicated that using DNA to adsorb THAQ from solution is a simple, effective, and affordable method with promising practical potential.

Looking ahead, this study paves the way for the rational design of high-performance biomaterials based on DNA intercalation. Inspired by the progress in functional materials for environmental applications,[9] future work will focus on optimizing the immobilization

of DNA on solid supports, engineering reusable and robust adsorption devices, and exploring the universality of this strategy for other planar aromatic pollutants. The ultimate goal is to translate this fundamental interaction into a practical and scalable technology for water purification.

Acknowledgments

None.

Funding

This work was supported by the National Natural Science Foundation of China (Grant Nos. 22265003 and 21966008).

Conflict of interest

The authors declare no conflicts of interest.

Author contributions

Conceptualization: Rongrong Zhang, Junsheng Li
Formal analysis: Rongrong Zhang, Junsheng Li, Liujuan Yan, Ji Ma
Investigation: Rongrong Zhang, Junsheng Li, Guoxia Huang
Methodology: Rongrong Zhang, Junsheng Li
Writing–original draft: Rongrong Zhang
Writing–review & editing: Junsheng Li

Availability of data

The relevant data for this study are not deposited in the relevant repository and will be covered in further relevant subsequent studies. Data will be made available upon reasonable request to the corresponding author.

References

1. Sebak M, Molham F, Greco C, Tammam MA, Sobeh M, El-Demerdash A. Chemical diversity, medicinal potentialities, biosynthesis, and pharmacokinetics of anthraquinones and their congeners derived from marine fungi: A comprehensive update. *RSC Adv.* 2022;12(38):24887-24921. doi: 10.1039/D2RA03610J
2. Wang P, Wei J, Hua X, *et al*. Plant anthraquinones: Classification, distribution, biosynthesis, and regulation. *J Cell Physiol.* 2024;239(10):e31339. doi: 10.1002/jcp.31063
3. International Working Group on the Evaluation of Carcinogenic Risks to Humans. Some chemicals present in industrial and consumer products, food and drinking-water. *IARC Monogr Eval Carcinog Risks Hum.* 2013;101:9-549.
4. Siraj MA, Jacobs AT, Tan GT. Altersolanol B, a fungal tetrahydroanthraquinone, inhibits the proliferation of estrogen receptor-expressing (ER+) human breast adenocarcinoma by modulating PI3K/AKT, p38/ERK MAPK and associated signaling pathways. *Chem Biol Interact.* 2022;359:109891. doi: 10.1016/j.cbi.2022.109916
5. Li CWY, Walters S, Müller JF, Orlando J, Brasseur GP. Contamination of tea leaves by anthraquinone: The atmosphere as a possible source. *Ambio.* 2023;52(8):1373-1388. doi: 10.1007/s13280-023-01858-9
6. Sendelbach LE. A review of the toxicity and carcinogenicity of anthraquinone derivatives. *Toxicology.* 1989;57(3):227-240. doi: 10.1016/0300-483X(89)90113-3
7. Liberman DF, Fink RC, Schaefer FL, Mulcahy RJ, Stark AA. Mutagenicity of anthraquinone and hydroxylated anthraquinones in the *Ames/Salmonella* microsome system. *Appl Environ Microbiol.* 1982;43(6):1354-1359. doi: 10.1128/AEM.43.6.1354-1359.1982
8. Chen Z, Yin J, Huang S, Lai K, Peng J, Lai W. Ligand engineering-based high-efficiency photothermal sensors powered sensitive lateral flow immunoassay platform. *Anal Chem.* 2025;97(36):15389-15398. doi: 10.1021/acs.analchem.5c02864
9. Zhang S, Zhou S, Liu H, Xing M, Ding B, Li B. Pinecone-inspired nanoarchitectured smart microcages enable nano/microparticle drug delivery. *Adv Funct Mater.* 2020;30(28):2001754. doi: 10.1002/adfm.202002434
10. Aleid SM, Hamad SH, Al-Dalali S. Treatment of antibiotic fermentation effluents using charcoal adsorption. *Asian J Water Environ Pollut.* 2025. doi: 10.36922/AJWEP025240198
11. Moussavi G, Mahmoudi M. Removal of azo and anthraquinone reactive dyes from industrial wastewaters using MgO nanoparticles. *J Hazard Mater.* 2009;168(2-3):806-812. doi: 10.1016/j.jhazmat.2009.02.097
12. Wang WK, Zhang YY, Wang AB, Yu ZB, Han MF, Yang YS. Electrochemical performance of 1,4,5,8-tetrahydroxy-9,10-anthraquinone as cathode material in lithium batteries. *Acta Phys Chim Sin.* 2010;26(1):47-50. doi: 10.3866/PKU.WHXB20100105
13. Mao ZQ, Rha H, Kim J, *et al*. THQ-xanthene: An emerging strategy to create next-generation NIR-I/II fluorophores. *Adv Sci.* 2023;10(18):2207702. doi: 10.1002/advs.202301177

14. Malik EM, Müller CE. Anthraquinones as pharmacological tools and drugs. *Med Res Rev.* 2016;36(4):705-748. doi: 10.1002/med.21391
15. Mueller SO, Stopper H. Characterization of the genotoxicity of anthraquinones in mammalian cells. *Biochim Biophys Acta.* 1999;1428(2-3):406-414. doi: 10.1016/S0304-4165(99)00064-1
16. Bondy GS, Armstrong CL, Dawson BA, Héroux-Metcalf C, Neville GA, Roger CG. Toxicity of structurally related anthraquinones and anthrones to mammalian cells *in vitro*. *Toxicol In Vitro.* 1994;8(3):329-335. doi: 10.1016/0887-2333(94)90153-8
17. Valduga AT, Gonçalves IL, Saorin Puton BM, de Lima Hennig B, de Brito ES. Anthraquinone as emerging contaminant: Technological, toxicological, regulatory and analytical aspects. *Toxicol Res.* 2023;40(1):11-21. doi: 10.1007/s43188-023-00202-3
18. Xie Q, Jiang D, Yong L, *et al.* Anthraquinone in Chinese tea: Concentration and health risk assessment. *Cogent Food Agric.* 2024;10(1):2293557. doi: 10.1080/23311932.2024.2321674
19. Routoula E, Patwardhan SV. Degradation of anthraquinone dyes from effluents: A review focusing on enzymatic dye degradation with industrial potential. *Environ Sci Technol.* 2020;54(2):647-664. doi: 10.1021/acs.est.9b03737
20. Ghaleb S, Yammine P, El-Nakat H, *et al.* Analysis of benzene, toluene, and xylene contaminants in the groundwater of Tripoli, Lebanon. *Asian J Water Environ Pollut.* 2025. doi: 10.36922/AJWEP025310239
21. Wang Y, Cui LH, Feng CL, Dong Z, Fan W, Peijnenburg WJGM. Taxon-toxicity study of fish to typical transition metals: Most sensitive species are edible fish. *Environ Pollut.* 2021;284:117501. doi: 10.1016/j.envpol.2021.117154
22. Chatterjee N, Walker GC. Mechanisms of DNA damage, repair, and mutagenesis. *Environ Mol Mutagen.* 2017;58(5):235-263. doi: 10.1002/em.22087
23. Hoeijmakers JHJ. Genome maintenance mechanisms for preventing cancer. *Nature.* 2001;411(6835):366-374. doi: 10.1038/35077232
24. Carr TH, McEwen R, Dougherty B, *et al*. Defining actionable mutations for oncology therapeutic development. *Nat Rev Cancer.* 2016;16(5):319-329. doi: 10.1038/nrc.2016.35
25. Zhang GW, Ma YD. Spectroscopic studies on the interaction of sodium benzoate, a food preservative, with calf thymus DNA. *Food Chem.* 2013;141(1):41-47. doi: 10.1016/j.foodchem.2013.02.122
26. Lerman LS. Structural considerations in the interaction of DNA and acridines. *J Mol Biol.* 1961;3:18-30. doi: 10.1016/S0022-2836(61)80004-1
27. Reynisson J, Schuster GB, Howerton SB, *et al.* Intercalation of trioxatriangulenium ion in DNA: Binding, electron transfer, x-ray crystallography, and electronic structure. *J Am Chem Soc.* 2003;125(8):2072-2083. doi: 10.1021/ja0211196
28. Malik MS, Alsantali RI, Jassas RS, *et al*. Journey of anthraquinones as anticancer agents - a systematic review of recent literature. *RSC Adv.* 2021;11(57):35806-35827. doi: 10.1039/d1ra05686g
29. Li JS, Feng Z, Wang JT, Huang G, Yan L. Interaction of aflatoxin G1 with free DNA *in vitro* and possibility of its application in removing aflatoxin G1. *J Environ Sci Health B.* 2021;56(10):932-940. doi: 10.1080/03601234.2021.1979838
30. Xiong YN, Li JS, Huang GX, Yan L, Ma J. Interacting mechanism of benzo(a)pyrene with free DNA *in vitro*. *Int J Biol Macromol.* 2021;167:854-861. doi: 10.1016/j.ijbiomac.2020.11.042
31. Huang GX, Li JS, Yan LJ, Ma J. Adsorption of 1,2-benzanthracene from aqueous solution by DNA-conjugated magnetic nanoparticles. *Water Air Soil Pollut.* 2022;233(1):14. doi: 10.1007/s11270-021-05476-7
32. Huang GX, Ma J, Li JS, Yan L. Removal of 1,2-benzanthracene via the intercalation of 1,2-benzanthracene with DNA and magnetic bead-based separation. *Nucleosides Nucleotides Nucleic Acids.* 2021;40(2):137-156. doi: 10.1080/15257770.2020.1839905
33. Gilad Y, Senderowitz H. Docking studies on DNA intercalators. *J Chem Inf Model.* 2014;54(1):96-107. doi: 10.1021/ci400352t
34. Panigrahi GK, Verma N, Singh N, *et al*. Interaction of anthraquinones of Cassia occidentalis seeds with DNA and glutathione. *Toxicol Rep.* 2018;5:164-172. doi: 10.1016/j.toxrep.2017.12.024
35. Liu HK, Sadler PJ. Metal complexes as DNA intercalators. *Acc Chem Res.* 2011;44(5):349-359. doi: 10.1021/ar100140e
36. Navas F, Mendes F, Santos I, *et al*. Enhanced cytotoxicity and reactivity of a novel platinum(IV) family with DNA-targeting naphthalimide ligands. *Inorg Chem.* 2017;56(11):6175-6183. doi: 10.1021/acs.inorgchem.7b00136
37. Raghuvanshi DS, Verma N, Singh SV, *et al.* Synthesis of thymol-based pyrazolines: An effort to perceive novel potent-antimalarials. *Bioorg Chem.* 2019;88:102934. doi: 10.1016/j.bioorg.2019.102933
38. Cai CQ, Chen XM, Ge F. Analysis of interaction between tamoxifen and ctDNA in vitro by multi-spectroscopic methods. *Spectrochim Acta A Mol Biomol Spectrosc.* 2010;76(2):202-206. doi: 10.1016/j.saa.2010.03.017
39. Pan HZ, Wang XM, Ding LS. Interaction mode between methylene blue-Pr(III) complex and herring-sperm

DNA. *Spectrosc Lett.* 2011;44(4):294-299.
doi: 10.1080/00387010.2010.523923
40. Tian ZS, Wang ZC, Han XX, *et al*. Study on the interaction between cannabinol and DNA using acridine orange as a fluorescence probe. *J Mol Recognit.* 2018;31(2):e2674.
doi: 10.1002/jmr.2682
41. Tian ZY, Cui HL, Liu H, *et al.* Study on the interaction between the 1,4,5,8-naphthalene diimide-spermine conjugate (NDIS) and DNA using a spectroscopic approach and molecular docking. *MedChemComm.* 2017;8(11):2079-2092.
doi: 10.1039/c7md00389g
42. Lien J, Bull T, Michelmore RW, Guo T. Fast fluorescence titration quantification of plasmid DNA with DNA attractive magnetic nanoparticles. *Anal Chem.* 2021;93(38):12854-12861.
doi: 10.1021/acs.analchem.0c04892
43. Cao Y, He XW. Studies of interaction between safranine T and double helix DNA by spectral methods. *Spectrochim Acta A Mol Biomol Spectrosc.* 1998;54A(6):883-892.
doi: 10.1016/S1386-1425(97)00277-1
44. Tan KL, Hameed BH. Insight into the adsorption kinetics models for the removal of contaminants from aqueous solutions. *J Taiwan Inst Chem Eng.* 2017;74:25-48.
doi: 10.1016/j.jtice.2017.01.024
45. Wibowo E, Rokhmat M, Abdullah M. Reduction of seawater salinity by natural zeolite (Clinoptilolite): Adsorption isotherms, thermodynamics and kinetics. *Desalination.* 2017;409:146-156.
doi: 10.1016/j.desal.2017.01.026
46. Omidinasab M, Rahbar N, Ahmadi M, *et al.* Removal of vanadium and palladium ions by adsorption onto magnetic chitosan nanoparticles. *Environ Sci Pollut Res Int.* 2018;25(34):34262-34276.
doi: 10.1007/s11356-018-3137-1
47. Huang S, Liang Y, Huang CS, *et al*. Systematical investigation of binding interaction between novel ruthenium(II) arene complex with curcumin analogs and ctDNA. *Luminescence.* 2016;31(7):1384-1394.
doi: 10.1002/bio.3119
48. Eryazici I, Yildirim I, Schatz GC, Nguyen ST. Enhancing the melting properties of small molecule-DNA hybrids through designed hydrophobic interactions: An experimental-computational study. *J Am Chem Soc.* 2012;134(17):7450-7458.
doi: 10.1021/ja300322a
49. Rehman SU, Sarwar T, Ishqi HM, Husain MA, Hasan Z, Tabish M. Deciphering the interactions between chlorambucil and calf thymus DNA: A multi-spectroscopic and molecular docking study. *Arch Biochem Biophys.* 2015;566:7-14.
doi: 10.1016/j.abb.2014.12.013
50. Mahanthappa M, Savanur MA, Yellappa S. Molecular interaction studies of zinc sulphide nanoparticles with DNA and its consequence: A multitechnique approach. *Luminescence.* 2021;36(1):45-56.
doi: 10.1002/bio.3912
51. Bag S, Bhowmik S. Fluorescence spectroscopy: A useful method to explore the interactions of small molecule ligands with DNA structures. *Methods Mol Biol.* 2024;2719:33-49.
doi: 10.1007/978-1-0716-3461-5_3
52. Dogra S, Awasthi P, Nair M, Barthwal R. Interaction of anticancer drug mitoxantrone with DNA hexamer sequence d-(CTCGAG)2 by absorption, fluorescence and circular dichroism spectroscopy. *J Photochem Photobiol B.* 2013;123:48-54.
doi: 10.1016/j.jphotobiol.2013.03.015
53. Favicchio R, Dragan AI, Kneale GG, Read CM. Fluorescence spectroscopy and anisotropy in the analysis of DNA-protein interactions. *Methods Mol Biol.* 2009;543:589-611.
doi: 10.1007/978-1-60327-015-1_35
54. Kashanian S, Khodaei MM, Pakravan P. Spectroscopic studies on the interaction of isatin with calf thymus DNA. *DNA Cell Biol.* 2010;29(10):639-646.
doi: 10.1089/dna.2010.1054
55. Ye YX, Liang JQ, She JL, *et al*. Two new alkaloids and a new butenolide derivative from the Beibu Gulf sponge-derived fungus *Penicillium* sp. SCSIO 41413. *Mar Drugs.* 2023;21(1):53.
doi: 10.3390/md21010027
56. He G, Wang WX, Zhou YX, Zhao G, Liao J. Ampholytic ion-exchange magnetic beads: A promising tool for selecting short fragments in circulating cell-free DNA analysis. *Front Oncol.* 2024;14:1423183.
doi: 10.3389/fonc.2024.1397680
57. Jiang ZK, Li JS, Huang GX, Yan L, Ma J. Common carp sperm chromatin as an economical and effective remover for benzo(a)pyrene from pollutants. *Heliyon.* 2024;10(12):e33137.
doi: 10.1016/j.heliyon.2024.e33137
58. Zhang J, Li JS, Huang GX, Yan L. Chromatin extracted from common carp testis as an economical and easily available adsorbent for ethidium bromide decontamination. *Heliyon.* 2022;8(6):e09560.
doi: 10.1016/j.heliyon.2022.e09565
59. Li JS, Wang XX, Feng Z, Huang G, Yan L, Ma J. Optimization of aflatoxin B1 removal efficiency of DNA by resonance light scattering spectroscopy. *Spectrochim Acta A Mol Biomol Spectrosc.* 2023;292:122390.
doi: 10.1016/j.saa.2023.122398
60. Ho YS, McKay G. Pseudo-second order model for sorption processes. *Process Biochem.* 1999;34(5):451-465.
doi: 10.1016/S0032-9592(98)00112-5
61. Ho YS, Ng JCY, McKay G. Kinetics of pollutant sorption by biosorbents: Review. *Sep Purif Methods.* 2000;29(2):189-232.

doi: 10.1081/SPM-100100009
62. Radia DN, Essa MS, Aljeboree AM, Jawad MA. Evaluation of the adsorption efficiency of biopolymer hydrogel nanocomposite/nanoclay in wastewater dye removal. *Asian J Water Environ Pollut.* 2024;21(4): 27-35.
doi: 10.3233/AJW240045
63. De Gisi S, Lofrano G, Grassi M, Notarnicola M. Characteristics and adsorption capacities of low-cost sorbents for wastewater treatment: A review. *Sustainable Mater Technol.* 2016;9:10-40.
doi: 10.1016/j.susmat.2016.06.002
64. Miklos DB, Remy C, Jekel M, *et al*. Evaluation of advanced oxidation processes for water and wastewater treatment - a critical review. *Water Res.* 2018;139:118-131.
doi: 10.1016/j.watres.2018.03.042